Correcting slice selectivity in hard pulse sequences

David Manuel Grodzki[1,2], Peter Jakob[1], and Bjoern Heismann[2,3]

[1]EP5, University of Wuerzburg, Wuerzburg, Bavaria, Germany, [2]Magnetic Resonance, Siemens AG, Erlangen, Germany, [3]Friedrich-Alexander-University, Erlangen, Germany

Introduction: Many MRI sequences use non-selective hard pulse excitation in the presence of imaging gradients. Examples are the BURST sequence [1] or the ultrashort echo time (TE) sequences zTE [2], WASPI [3] and PETRA [4]. Ultrashort TE imaging offers new application for MRI, as tissues like bone, tendons, ligaments or teeth provide signal and can be evaluated. Because the imaging gradients are non-zero during the pulse, the excitation in these sequences is not truly non-selective. A slice that is defined by the spectral profile of the pulse is excited, as it is shown in Fig. 1. The excited slice does not only rotate while different radial projections are acquired, but also changes its thickness if the gradient strength is changed.

In this work, we investigate possible artefacts due to unwanted slice-selectivity in hard pulse sequences. A post-processing algorithm is presented that eliminates slice selection artefacts as long as the imaged object fits into the sphere defined by the first minimum of the excitation profile.

Theory: During the acquisition of k-space values, the spectral profile of the pulse *P(ω(x),k)* superposes the magnetization distribution *f(x)*. The disturbed k-space $F'(k) = \sum f(x)P(x,k)e^{ikx}$ **(1)** is measured. If *F'(k)* is Fourier back transformed, the disturbed image *f'(x)* is calculated.

We propose to solve the influence of the excitation profile by using matrix inversions instead of Fourier back transformations. Defining the matrix $D_{kx} = P(x,k)e^{ikx}$ **(2)**, Eq. (1) can be rewritten as the matrix equation $F'_k = D_{kx} f_x$ **(3)**, where F'_k is the disturbed k-space measured in the MRI scan. The elements of D_{kx} are known and can be calculated. They depend on the gradient trajectories and timings of the specific sequence, pulse profiles, resolution and FOV. The system of linear equations in Eq. (3) can be solved by a matrix inversion $f_x = D_{kx}^{-1} F'_k$ **(4)** and the undisturbed image is obtained.

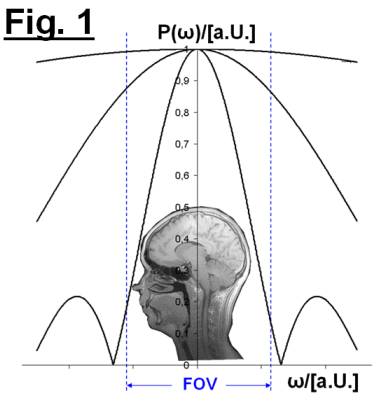

Materials and Methods: Without loss of generality, the problem was evaluated for the PETRA sequence. We used Eq. (1) to simulate the disturbed k-space *F'(k)* and disturbed image *f'(x)* of a two-dimensional object. Using Eq. (4), the corrected image *f(x)* was calculated from the disturbed k-space. The pulse duration was set to τ=14 µs and different maximum gradient strengths (4-20 mT/m) were simulated for a FOV of 300 mm, matrix size N = 250 and TE = 70 µs.

The PETRA sequence was implemented and tested on a 3T clinical scanner. Data post-processing and image reconstruction was implemented and performed in-line. By using the radial symmetries of the problem, the 3D data correction can be performed mainly in 1D and possible buffer limitations are avoided. For all measurements we used a τ=14 µs hard pulse. In-vivo head experiments were performed on healthy volunteers after informed consent. Gradient strengths from 8.6 to 17.2 mT/m were used while all other parameters were kept constant. The measurements were reconstructed with and without the application of the correction algorithm. P_{min} is defined to be the minimum of *P(x,k)* within the FOV. r_0 is the distance from image center to the first minimum of *P(x,k)*.

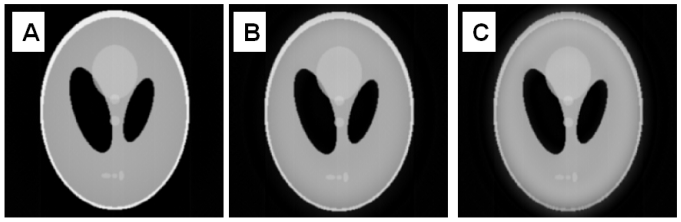

Fig. 2: Simulation of a disturbed 2D image f'(x) for the maximum gradient strengths 8, 12, and 16 mT/m from A to C. The corrected images (not shown) do not show any differences compared to the original image f(x).

Results: Simulations of the disturbed 2D object are presented in Fig. 2. No differences are detectable between the original object and the corrected image. Uncorrected and corrected in-vivo head images obtained with different gradient strengths are presented in Fig. 3. For the simulations and measurements, r_0 lies outside of the FOV for G_{max} < 11,2 mT/m. In the simulations, r_0 lies at 139.8 and 104.9 mm for 12 and 16 mT/m, respectively, and at 111.5 mm for 15.05 mT/m in the measurements.

Discussion: In sequences with non-zero gradients during the RF pulse, the excitation is not perfectly non-selective, but depends on both the k-space and image-space point values. For smaller gradients, where r_0 is outside of the object, this leads to intensity errors in the outer parts as well as slight blurring. This can be seen in both the simulation and the in-vivo measurement, Figs. 2B and 3B. For higher gradients, severe blurring artefacts in the outer image parts occur, see Figs. 2C and 3C. The proposed correction algorithm recovers the influence of the excitation within the post-processing by matrix inversion. Using our correction approach, the influences of the spectral excitation profile can be completely eliminated in the simulation experiments. In the MR measurement data, the correction is proven as well, but limitations are found. The minimum of the excitation profile should be outside of the object as the noise level is increased close to minimal excitations, see Fig. 3F. The correction algorithm presented here for the PETRA sequence can easily be adapted for other sequences with non-zero gradients during excitation like zTE or WASPI. It can also be used for non-selective sequences with non-zero gradients during excitation like the BURST sequence.

In conclusion, we have shown the influence of the excitation profile in hard pulse non-selective excitations in the presence of gradients and have presented an approach to eliminate artefacts in post-processing. Enhanced contrast is enabled and blurring can be eliminated. The limits of our approach have been investigated. Higher readout bandwidths or longer pulses with higher flip angles are enabled with our approach. This might help to establish this sequence class in clinical applications.

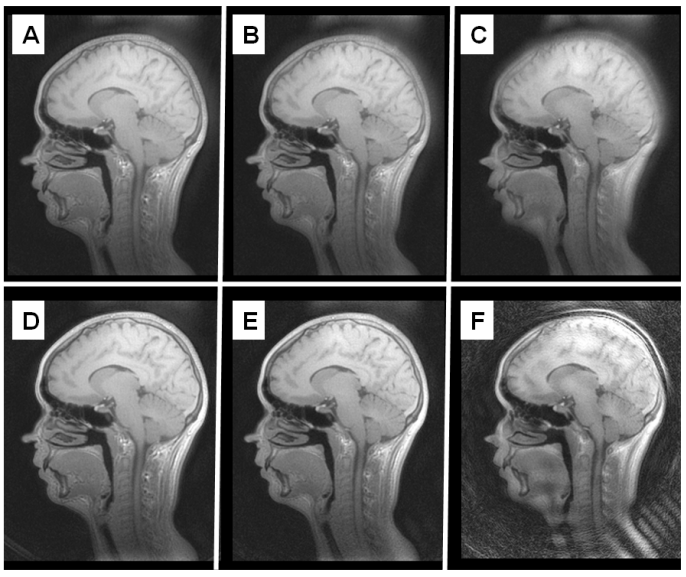

Fig. 3: In-vivo head images without (A-C) and with correction (D-F) with Gmax = 8.6 (A,D), 10.75 (B,E) and 15.05 mT/m (C,F). Images have identical windowing.

References: [1] Hennig et al. MAGMA 1993; [2] Weiger et al. MRM 2011; [3] Wu et al. JMRI 2010 ; [4] Grodzki et al. MRM 2011